Sensors & Actuators: A. Physical 347 (2022) 113959

Contents lists available at ScienceDirect

Sensors and Actuators: A. Physical

journal homepage: www.journals.elsevier.com/sensors-and-actuators-a-physical

Simultaneous measurement of microscale fluid viscosity, temperature, and velocity fields by tracking Janus particle on microparticle image velocimetry

Jhih-Cheng Wang [a,b,c], Wei-Long Chen [d], Chun-Jui Chen [d], Chun-Chieh Chang [d], Tai-Hua Yang [d,e], Han-Sheng Chuang [d,f,*]

[a] Division of Urology, Department of Surgery, Chi Mei Medical Center, Tainan 71004, Taiwan
[b] Medical Education Center, Chi Mei Medical Center, Tainan 71004, Taiwan
[c] Department of Electrical Engineering, Southern Taiwan University of Science and Technology, Tainan 71004, Taiwan
[d] Department of Biomedical Engineering, National Cheng Kung University, Tainan, Taiwan
[e] Department of Orthopedic Surgery, National Cheng Kung University Hospital, Tainan, Taiwan
[f] Medical Device Innovation Center, National Cheng Kung University, Tainan, Taiwan

ARTICLE INFO

Keywords:
Diffusometry
μPIV
Janus particle
Temperature
Viscosity
Velocity

ABSTRACT

Multifunctional sensing capability enables a comprehensive understanding of the unknown target to be measured. Given that fluid viscosity, temperature, and velocity fields are usually coupled parameters in a system, simultaneous measurement of the three environmental factors can prevent cross-talk and improve reliability. However, the task is apparently challenging because of the microscale targets. A technique combining microparticle image velocimetry and Janus particles was developed in this study to address such demand. With the rotational diffusivity and particle trajectories measured by the proposed technique and an empirical water-based viscosity-temperature relationship, the three unknown variables in a microfluidic environment were solved. The blinking frequency was derived using the Hilbert Huang Transform. Compared with those in a static and uniform temperature field, the measured data had good agreement with the predicted values. However, the agreement was impaired when the heating rate exceeded 0.34 °C/s. The optimal temperature range was found between 10 °C and 40 °C in the water-based solution. For a steady-state and nonuniform temperature field, two-dimensional (2D) numerical simulations of three linear temperature gradients were also studied. Results showed that the deviation increased as the temperature gradient increased or was near the low-temperature region. The same procedure was eventually applied to a real thermophoretic flow induced by an IR laser in a microchip. The 2D fluid viscosity, temperature, and velocity fields in the microchip were successfully obtained by tracking 10 particles. The potential of the approach provides insight into understanding some microfluidic applications with mild changes in temperature or creeping flow.

1. Introduction

Microparticle image velocimetry (μPIV) has been well known as a powerful flow visualization tool at the microscale since its introduction in 1998 [1,2]. Contrary to other microflow sensors that can only yield bulk measurement, the μPIV enables the studies of two-dimensional (2D) microflow with a detailed velocity distribution in various miniaturized fluid components, such as inkjet printer heads [3], micronozzles [4], and microchips [5–7]. With little modification, the velocity field can be used to derive other important parameters, such as pressure [8,9], vorticity [10,11], temperature [12], viscosity [13,14], and force [15,16]. However, abovementioned whole field measurements at the microscale are quite difficult to determine using current microfluidic sensors, such as the free standing pressure sensor [17], shear stress sensor [18], or hot-wire temperature sensor [19]. Yu et al. [20]. once attempted to measure the acoustic pressure around a single bubble by using PIV. They used a formula to convert the velocity component into pressure contours. The method revealed that a high-pressure region was formed on top of the bubble near a rigid boundary but at the bottom of the bubble near an elastic boundary, indicating the bubble migration is

* Correspondence to: BMOEMS Lab, Department of Biomedical Engineering, College of Engineering, National Cheng Kung University, Tainan 701, Taiwan.
E-mail address: oswaldchuang@mail.ncku.edu.tw (H.-S. Chuang).

https://doi.org/10.1016/j.sna.2022.113959
Received 31 July 2022; Received in revised form 9 September 2022; Accepted 18 October 2022
Available online 20 October 2022

dominated by the Bjerknes and buoyancy forces. Pramod et al. [21]. presented a diffusion-based temperature measurement on a μPIV system. Information on the temperature can be simply obtained according to the Brownian motion by analyzing the broadening of the correlation function from a pair of particle images. A range of temperatures from 20 °C to 80 °C was carefully calibrated, and the average discrepancy reached nearly ± 2.6 °C. However, the change in viscosity was not considered in the determination of temperature. In addition, the technique was susceptible to a flowing fluid. Charogiannis et al. [22]. proposed a unique device, known as thermographic particle velocimetry, to simultaneously measure interfacial temperature and velocity by simply incorporating an IR camera into a PIV system. The temperature was changed from 20 °C to 80 °C. The deviation was estimated to be approximately ± 1 °C at 80 % confidence level for this system. However, the measurable temperature was limited to the very near-surface region. Furthermore, the particle images for velocity should be visualized under an open channel because of the IR camera. Then, Chen et al. [23]. successfully developed a microviscometer by using the μPIV-based diffusometry. The fluid viscosities from 0.8 cP to 575 cP were determined by measuring the blinking frequency out of Janus particles suspended in a small drop of 2 μL. The measured and predicted data appeared to show good agreement, implying the potential of the technique for microviscometry. Despite the advanced progresses in extending the capabilities of the current μPIV, temperature and viscosity remain coupled with each other. This limitation affects the accuracy of measurement. To address this challenge, Chen et al. [24]. proposed a self-compensated algorithm to eliminate the environmental noises from temperature and viscosity by tracking the Janus particles. Given that the same Janus particles can yield both translational and rotational diffusivities, the particle diameter can be precisely estimated from the ratio of the both diffusivities by using Stokes-Einstein and Stokes-Einstein-Debye relations. The algorithm was then used to perform highly stable and sensitive immunosensing of a small biomolecule, i.e., IFN-γ, in a biological medium. The limit of detection (LOD) reached 0.45 pg/mL, because the uncertainties resulting from the background viscosity and temperature were immensely reduced. Based from our previous work, we hereby formulated a similar approach by tracking Janus particles for three simultaneous field measurements. The dynamic viscosity and temperature where each Janus particle was located could be estimated using the empirical viscosity–temperature relationship derived from the exponential curve fitting for the experimental data and the Stokes-Einstein-Debye relation. The blinking signal of Janus particles contained major information relevant to their local temperature and viscosity. The real-time frequency was extracted out of the blinking signal using the Hilbert-Huang transform (HHT). However, surface plasma resonance (SPR), response time, and the built-in defects in HHT caused discrepancies between the ideal and actual measurements. In addition, for the particle motion, conventional PIV using the cross-correlation algorithm was applied to a series of instantaneous particle image frames. Therefore, the 2D velocity field was obtained. Instead of point or bulk measurement, this approach features simultaneous whole field measurements for three common parameters, hence improving inaccuracy resulting from the cross-talk. The results suggested that the optimal temperature response time and temperature gradient should be maintained under 0.35 °C/s and 0.02 °C/μm, respectively. In addition, the approach was found suitable within a small temperature range between 10 °C (1.43 mPa s) and 40 °C (0.65 mPa s) in a static and uniform medium. Serious internal flow occurred when the temperature rose above 40 °C, but the glass window was covered with frost when the temperature dropped below 10 °C. The technique could eventually promote the fundamental understanding of some microfluidic applications with mild changes in temperature or creeping flow.

2. Methods and materials

2.1. Fabrication of Janus particles

Janus particles are good sources to provide essential information of rotational diffusivity and particle trajectory. Local parameters, such as viscosity, temperature, and velocity, around the particle can be revealed by tracking each particle. To fabricate the desired Janus particles, fluorescent polystyrene (PS) particles (1 μm; F13083, Thermo Fisher Scientific, USA) were first mixed with 95 % ethanol to make a final particle concentration of 0.1 % solids. The diluted suspension was then spread over a glass slide by drop deposition to form a single layer of particles. The highly pure ethanol and low-particle concentration promoted rapid evaporation to prevent serious agglomeration. After completely dried, a 30-nm gold film was coated on the surface of the PS particle by an e-beam evaporator with a deposition rate of 1 Å/s. The coated particles were collected from the glass slide by sonication for 5 min. High coating rate was used to facilitate the collection of particles from the glass slide. The collected colloidal suspension was purified five times using a filter disk (pore size: 3.2 μm) to remove particle aggregates and other impurities. The final concentration of the colloidal suspension was readjusted to 2×10^6 particles/mL by using deionized water plus 0.1 % Tween-20. The complete Janus particle appeared with one hemisphere opaque (covered with gold) and the other hemisphere was free for emission of fluorescence.

2.2. Experimental setup

Given that the major driving mechanism only relies on Brownian motion, the measurement setup can be simplified (Fig. 1). For regular measurement, unless mentioned otherwise, a 2-μL drop of Janus particle suspension was pipetted onto a glass slide and then topped with a cover glass. A 110-μm spacer made of 3 M tapes was used to separate the glass slide and the cover glass. To modulate the ambient temperature, a thermoelectric cooler (TECI-7103, T-Global, Taiwan) was adhered to the top cover glass with a thermal glue spread in between. The entire measurement assembly was positioned on the stage of an inverted epi-fluorescent microscope (IX71, Olympus, Japan) equipped with a 40 × objective and a filter cube (Ex: 530–550 nm/Em: 575-UF nm) specialized for the Janus particles. A digital CMOS camera (BFS-U3-31S4C-C, Point Grey, USA) was installed at the output side port of the microscope for fast image acquisition. Two scenarios, i.e., high viscosity along with low temperature or low viscosity along with high temperature, were expected to be measured by the system. In the case of high viscosity/low temperature, the Janus particle tended to yield low diffusivity, which resulted in a slow blinking signal. By contrast, in the case of low viscosity/high temperature, the Janus particle tended to yield high diffusivity, which resulted in a rapid blinking signal. The signal converted into frequency was then used to estimate the unknown viscosity and temperature.

2.3. Determination of blinking frequency by HHT

The rotational diffusivity measured from the Janus particles was expressed in terms of blinking frequency. In the absence of gradient in temperature or viscosity in the fluid, the temperature and viscosity distributions would be homogeneous, resulting in equal diffusivity everywhere in the medium. In this case, the blinking frequencies of all Janus particles are theoretically the same. Therefore, the frequency is independent of location and time (Fig. 2A). A precise frequency can therefore be obtained by averaging values over a large number of particles. Conversely, the even diffusivity will be disrupted when a gradient in temperature or viscosity occurs in the medium. In this case, the frequency becomes a function of location and time. The time effect is neglected when the flow reaches steady-state. The blinking frequency varies, because a particle may move across different viscosity and

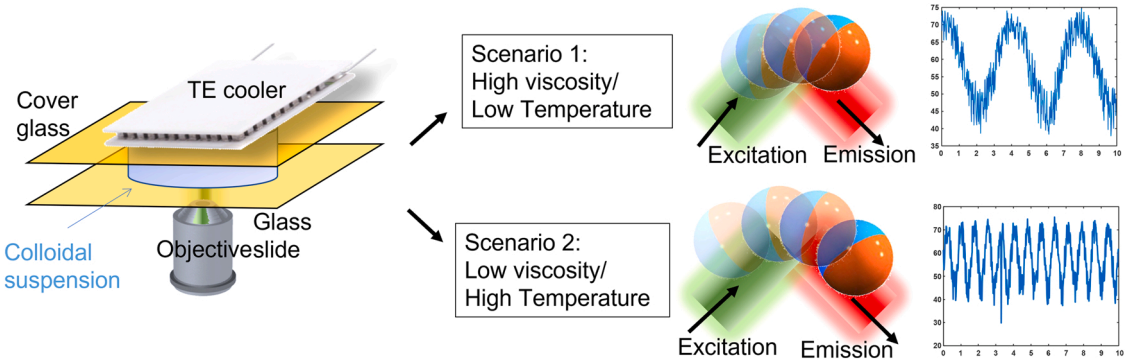

Fig. 1. Schematic of the experimental setup of the microparticle image velocimetry-based diffusometry. The blinking signals depicted two common scenarios observed in most experiments.

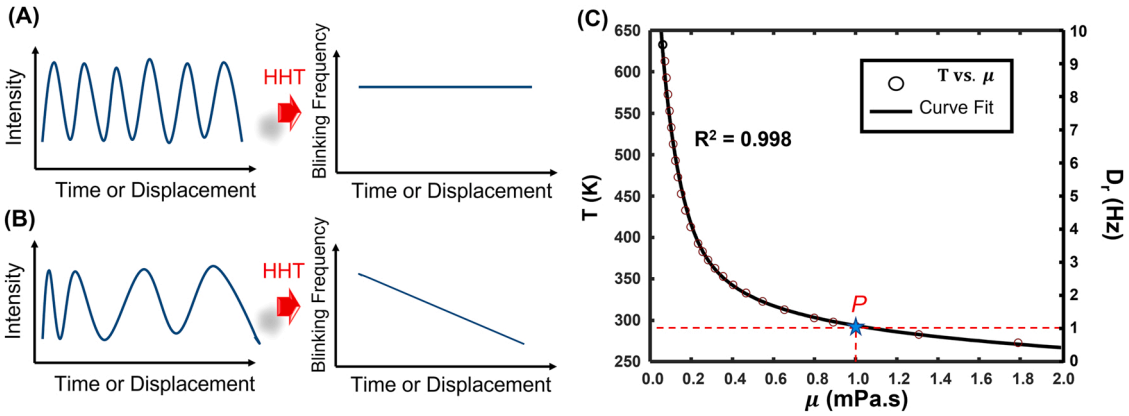

Fig. 2. Blinking signals and corresponding frequency spectra (A) with and (B) without background flow. (C) Rotational diffusivity in relation to the corresponding temperature and viscosity. *P* represents a point on the curve and its corresponding values in terms of blinking frequency, temperature, and viscosity.

temperature zones with the background flow (Fig. 2B). Hence, tracking each particle becomes vital, because none of the particles will yield the same rotational diffusivity. To extract the frequency out of a nonuniform sinusoidal wave, HHT provides an ideal method to address such kind of signal point by point. A decent frequency plot with respect to location can be obtained. The detailed information of extracting frequency out of a blinking signal by HHT can be referred to our prior literature [24]. In short, the raw blink signal (wavy intensity data) will be decomposed into intrinsic mode functions (IMFs) in the first step. Next, the highest correlated function will be selected among all the IMFs. Then, the selected IMF will be converted into a HHT frequency spectrum. To prevent the intrinsic defect in HHT, the first and the last 50 frames are truncated in advance. Finally, the varying frequency with respect to location can be obtained from the spectrum. By repeatedly analyzing each Janus particle along its trajectory on the map, a 2D frequency distribution can be plotted. The plot will eventually serve as an input to determine the final 2D viscosity and temperature fields.

2.4. Determination of viscosity, temperature, and velocity

The approach for deriving the viscosity and temperature was based on both the empirical viscosity-temperature relationship (Eq. (1)) and the Stokes-Einstein-Debye relation (Eq. (2)). The empirical viscosity–temperature relationship is a self-derived fitting curve for water with two exponential terms. The experimental data were referred to the prior literature [25], and the R^2 value of the fitting curve reached nearly 99.8 %. However, for nonwater-based solutions, a new fitting curve will need to be considered. In addition, the fluid velocity was derived from the particle motion between a pair of particle images using the conventional cross-correlation algorithm. Thus, Janus particles were used herein to provide experimental blinking signals and particle trajectories. The blinking signal corresponding to the rotational diffusivity was expressed in terms of frequency. Given the particle diameter, the two independent equations (Eqs. (1) and (2)) could be correlated to solve the two unknown variables (μ and *T*) (Fig. 2C).

$$\mu = 23.12 \quad exp\left(-\frac{T}{27.856}\right) + 0.0028 \quad exp\left(-\frac{T}{151.52}\right) \tag{1}$$

$$\mu = \frac{k_B T}{D_r \pi d_p^{\,3}} \tag{2}$$

Where μ and *T* are the fluid viscosity and temperature, respectively; d_p denotes the particle diameter (1 μm in this study); D_r is the rotational diffusivity; and K_B denotes the Boltzmann constant. Given that each particle provides the information of local viscosity and temperature, the 2D viscosity and temperature distributions can be separately plotted by tracking all Janus particles and analyzing their blinking signal along their trajectories. By contrast, the velocity field can be derived from a pair of particle images by using the conventional PIV approach. Particles are very likely to migrate and experience multiple temperature and viscosity zones when a temperature gradient or a viscosity gradient is formed. Thus, the flow field to be measured should be maintained in a steady state.

3. Results and discussion

3.1. Characterizations of Janus particle responses to modulated temperature

Prior studies [26] have stated that gold coating is likely to show local SPR when irradiated by light centered at its absorption peak (520–550 nm). The effect was also observed in the measurement when the incident light was green due to the optical filter (530–550 nm) (Fig. 3A). The medium temperatures between pure PS particles (control) and Janus particle were carefully compared using a temperature-sensitive dye, Rhodamine B (83689, Merck, Darmstadt, Germany) (Fig. 3B). The intensity difference in the region of interest was evidently revealed in the profile. A slight increase of 4.8 °C was measured, implying that correction was needed to reflect the true value. For a dynamic measurement (Fig. 3C), the preset temperature was modulated by a TE cooler that adhered to the top cover glass. A thermocouple was placed next to the suspension droplet to indicate the real-time temperature. The temperature difference between the droplet and the thermocouple was calibrated in advance. Three heating modes were investigated. In heating mode 1, the droplet was heated from 27 °C to 43 °C by the TE cooler in 47 s. In heating mode 2, the droplet was slowly heated from 27 °C to 43 °C by 11 steps, and the temperature was maintained in each step for 14 s. In the heating mode 3, the droplet was also slowly heated from 27 °C to 43 °C by 11 steps, but the temperature was maintained in each step for 21 s. The results showed that the measured and predicted values were in better agreements in heating modes 2 ($R^2 = 0.95$) and 3 ($R^2 = 0.96$), whereas a large discrepancy was observed in heating mode 1. Notably, the slight shifts between the predicted and the measured data in modes 2 and 3 are likely due to the bulk probe size of the thermocouple. Instead of a point measurement, the probe appeared to form a source of interference to its environment. The serious lag in mode 1 suggested that the heating rate may have exceeded the response time of the Janus particles. The final stage of the experimental data stopped increasing, because the TE cooler power was turned off at the end of the mode. The response time of the current Janus particles was then estimated to be below 0.34 °C/s. Conversely, a static measurement was apparently free from the limitation of heating rate. With preset droplet temperatures at 10 °C, 20 °C, 25 °C, and 40 °C, the measured temperature (Fig. 3D) and viscosity (Fig. 3E) from the Janus particles showed good agreements with their predicted counterparts. The predicted viscosity curve (solid line in Fig. 3E) was plotted as a function of temperature based on the empirical viscosity-temperature relationship in water (Fig. 2C). Temperature higher than 40 °C was prone to induce nonuniform internal flow, while temperature lower than 10 °C caused serious condensation that obstructed observation. Hence, the optimal temperature range for this approach was within 10 °C and 40 °C. In Fig. 3C–E, the error bars represent one standard deviation of uncertainty. Each error bar in Fig. 3C is a result of 10 independent Janus particles while that in Figs. 3D and 3E is a result of at least 100 independent Janus particles. The data points represent mean values.

3.2. Evaluation of simulated flow under a temperature gradient

A complex case may occur when a temperature gradient is formed due to inhomogeneous heating. To evaluate the capability of the proposed approach in this special case, a thermophoretic flow induced by a point heat source in a droplet sandwiched between a top cover glass and a bottom glass slide was investigated by numerical simulation using COMSOL Multiphysics®. Two simulation modules, namely, laminar flow and heat transfer in fluids, were employed in the 2D axisymmetric model (Fig. 4A). The point heat source was fixed at the center of the axisymmetric model. To study the impact of the flow speed on the blinking signal of Janus particles, three heating temperatures (i.e., 25 °C, 33 °C, and 40 °C) were investigated. In the laminar flow module, no-slip boundaries were set on the upper and lower walls, while the free surface on the right side of the droplet was set to be symmetric. In the heat transfer in the fluid module, the top and bottom walls in contact with the glasses, except the heat source, were set to have a convective heat flux of 2 W/(m^2 K). The right-side free surface was set to be the same as the ambient temperature (20 °C). A physics-controlled mesh with a normal element size was used on the whole model. The simulation was performed under the time-dependent mode for 5 s. The velocity and temperature surface contours after reaching the steady-state are demonstrated in Figs. 4B and 4C, respectively. The results indicated that a stable poloidal vortex was created by the thermophoretic flow. To verify the temperature distribution in space by using our approach, the blinking signal along the A-A′ axis was analyzed. The simulated blinking

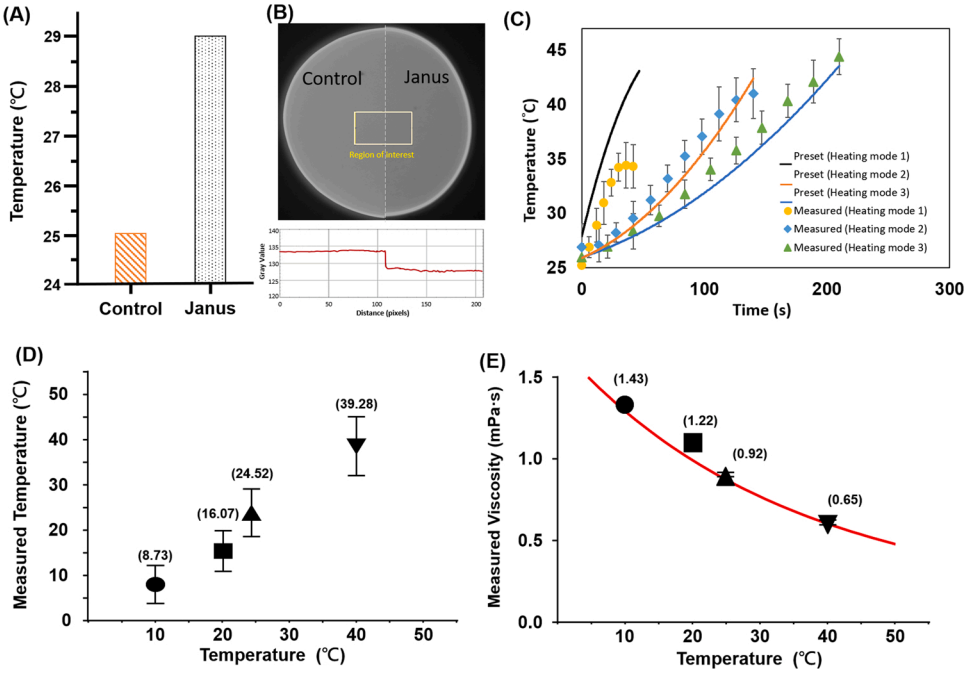

Fig. 3. Characterizations of Janus particle responses to temperature modulations. (A) Temperature increase due to the surface plasma resonance effect. (B) Comparison of the temperature zones in the control and the Janus particle groups irradiated with green light. The plot below the image shows the intensity profile of Rhodamine B in the yellow rectangular region of interest. (C) Dynamic temperature measurements under three heating modes (n = 10 particles). The error bars represent one standard deviation of uncertainty. (D–E) Comparisons of measured and predicted temperatures and viscosities in a static medium (n > 100 particles). The numbers in the parentheses are mean values of temperature and viscosity. The error bars represent one standard deviation of uncertainty.

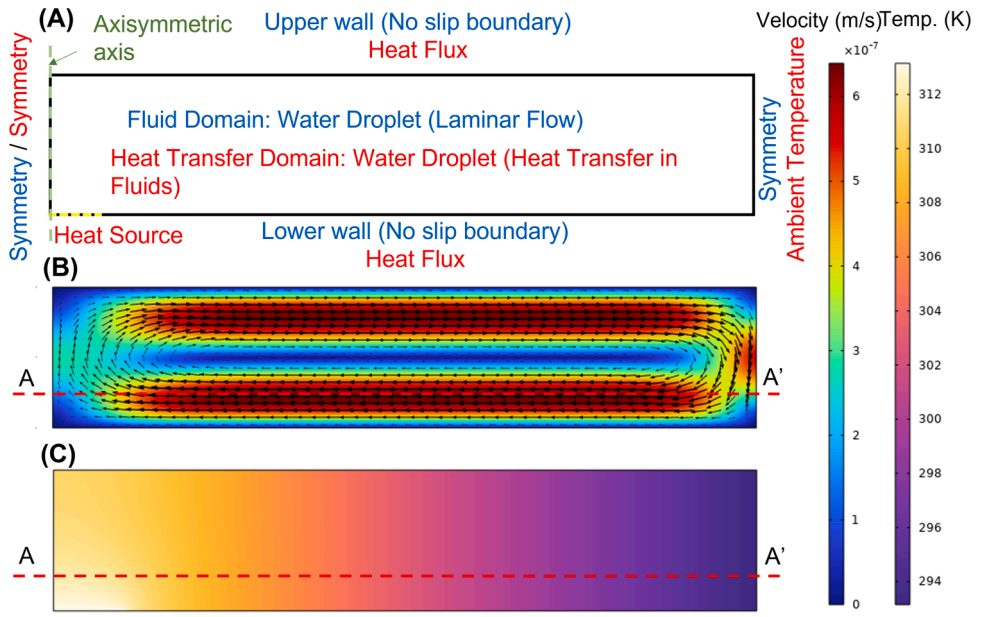

Fig. 4. (A) Simulation model composed of the laminar flow and the heat transfers in fluid modules. (B) Simulated steady-state velocity contours under a heat source of 25 °C. (C) Simulated steady-state temperature contours under a heat source of 25 °C.

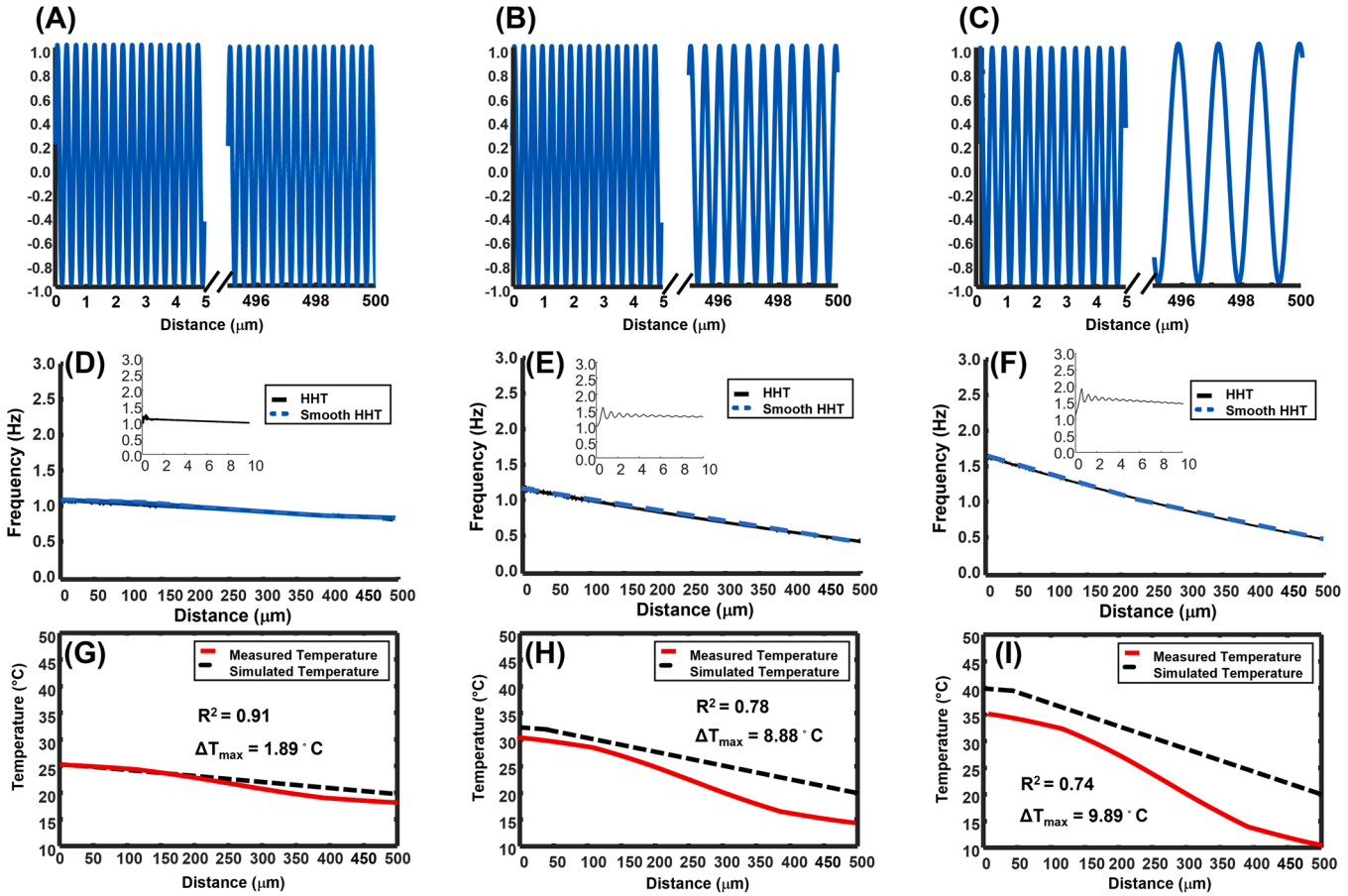

Fig. 5. Simulation results for three temperature gradients. (A–C) Raw blinking signals generated at 25 °C, 33 °C, and 40 °C. (D–F) Hilbert-Huang transform (HHT) frequency spectra obtained from the blinking signals at 25 °C, 33 °C, and 40 °C. The insets show the fluctuations in the raw HHT frequency spectra. The blue curves denote the smoothed lines. (G–I) Final temperatures of the measured (red solid line) and predicted (black dotted line) data.

signal (I) was generated depending on its horizontal velocity, location, and temperature based on the following sinusoidal equation:

$$I = sin(2\pi D_r t), \quad (3)$$

where t is the elapsed time. The duration was defined as the total length (500 μm) divided by the horizontal velocity. For simplification, the horizontal velocity was determined to be the maximum velocity (V_m) under each temperature gradient. D_r is a function of temperature and viscosity determined by its location ($s = V_m t$) along the A-A′ axis. The simulated sinusoidal waves at 25 °C (Fig. 5A), 33 °C (Fig. 5B), and 40 °C (Fig. 5C) were therefore generated. The potential SPR effect and lag due to the low response time were neglected in the simulation. After separately analyzing the simulated blinking signals with HHT, their corresponding HHT frequency spectra along the A-A′ axis were depicted (Fig. 5D–F). The rugged frequency spectra were later smoothed by a moving average filter. The final temperatures along the A-A′ axis were estimated by substituting the location-dependent frequencies and viscosities into the Stoke-Einstein-Debye relation (Fig. 5G–H). Among the three diagrams, the lowest temperature gradient (20–25 °C) apparently showed a better result than the other two counterparts. When the temperature gradient increased, the measured blinking frequency tended to deviate away from the predicted line, especially in the low-temperature zone. A high temperature gradient induces a high vortex, leaving the Janus particles less time to respond to the environmental change. At high temperature, the blinking signal waves were dense, but the waves turned sparse toward a low temperature. Accordingly, the sparse signal waves resulted in a significant deviation because of a poor resolution for HHT. The trends suggested that a high temperature gradient should be avoided to ensure the accuracy of measurement.

3.3. *Experimental 2D viscosity, temperature, and velocity fields generated from the actual thermophoretic flow*

The previous simulation laid a good foundation for measuring the actual thermophoretic flow. A Janus particle suspension (2 μL) was first sandwiched between two glass slides separated with a gap of 110 μm (Fig. 6A). The bottom glass slide was coated with a 150 μm Au/30 nm Cr film on the surface to absorb the incident light energy. The device was placed on an upright microscope (IX51, Olympus, Japan). The heat was generated from the 300-mW infrared (IR) laser (1064 nm; LD-WL206, Optoelectronics Tech., Taiwan) that irradiated the bottom glass slide. A poloidal vortex was driven by the IR-generated thermal gradient. The particle images were recorded with a 40 × objective from a digital camera on the top of the device. To avoid strong out-of-plane motion, the focal plane was positioned approximately 28 μm above the bottom glass slide where the Janus particles apparently migrated toward the center of the droplet with the background flow induced by the thermophoresis (Video S1) when the IR laser was on. Given 1-μm Janus particles and a 40 × objective, the depth of correlation [27] was estimated to be 1.65 μm. Therefore, the vertical thermal gradient imposed negligible influence on the measurement. To reconstruct three-dimensional temperature and viscosity contours, vertical scanning will need to be implemented under a steady-state flow condition. A PIV velocity map was obtained, with 500 consecutive image frames, an interrogation window of 64 × 64 pixels, 50 % overlap, and a time interval of 40 ms (Fig. 6B). The gray region at the center of the image indicated the irradiated spot of the IR laser. In general, the map showed that the overall flow moved toward the center, while the laser was on. The mean velocity reached nearly 1.8 μm/s. Ten particles were tracked starting from the periphery and ending near the central region (Fig. S1), and their blinking signals were converted to the HHT spectra to estimate the corresponding temperatures and viscosities along their trajectories (Fig. S2). After combining their temperatures and viscosities and filling out the vacancies between particles by interpolation, the 2D temperature and viscosity fields of the thermophoresis were obtained (Figs. 6C and 6D). The central temperature was as high as 33.2 °C, while the peripheral temperature remained low at 27.4 °C. A concentric viscosity gradient was also formed in relation to the temperature gradient at the same time. The fluid viscosity in the central region dropped from 0.89 mPa s to nearly 0.68 mPa s. The spatial resolution could be improved by tracking more particles. However, the time consumption may pose a major barrier, because the analysis of each particle track took up to 4 h. Nevertheless, the approach still demonstrated the great potential of simultaneous measurement of microscale fluid viscosity,

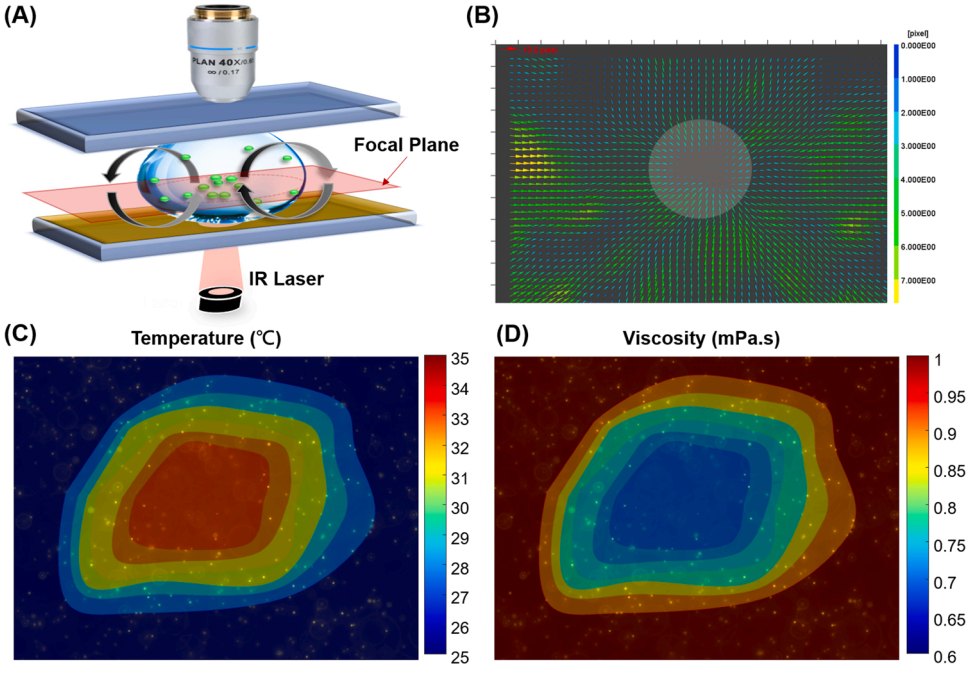

Fig. 6. Measurement setup of the thermophoretic flow in a sandwiched water droplet. (A) Schematic of the experimental setup. The heat source is provided by the infrared laser. The particle images were recorded on the focal plane located 28 μm above the bottom glass slide. (B) Whole field velocity measurement. The fluid velocity is indicated by arrows. (C–D) 2D temperature and viscosity fields in the vicinity of the heat source.

temperature, and velocity fields in some complex flow environments.

Supplementary material related to this article can be found online at doi:10.1016/j.sna.2022.113959.

4. Conclusions

The μPIV is a well-established platform for exploring various microfluidic devices after having been rapidly developed over the past decades. The whole field measurement imparts μPIV its unique capability of investigating the comprehensive details of microflow. This study carefully combined μPIV with Janus particles and then simultaneously measured 2D microscale fluid viscosity, temperature, and velocity fields by tracking the particles. The viscosity and temperature were derived from the empirical viscosity–temperature relationship and the Stokes-Einstein-Debye relation. The velocity was derived alone based on the conventional cross-correlation algorithm. The rotational diffusivity in terms of frequency was extrapolated from the blinking signal based on the HHT algorithm. Compared with the preset temperatures, the heating rate was suggested to be kept below 0.34 °C/s. The measured and predicted values were in good agreement when the temperature field was uniform and constant. The temperature to be measured by the proposed approach should be between 10 °C (0.89 mPa s) and 40 °C (0.68 mPa s), because temperatures higher than 40 °C and lower than 10 °C induced nonuniform internal flow and caused serious condensation that obstructed observation, respectively. In addition, poloidal microflow induced by a temperature gradient was evaluated by simulation and experimentally. The simulation results suggested that uncertainty appeared to deteriorate as the temperature gradient increased. The temperature difference should be no more than 10 °C to prevent significant deviations. To the best of our knowledge, we have study successfully developed an approach with 2D multi-functional sensing capabilities for viscosity, temperature, and velocity on the basis of μPIV. The multifunctional sensing capabilities were believed to promote the understanding of some microfluidic devices with mild changes in temperature or creeping flow.

CRediT authorship contribution statement

Jhih-Cheng Wang & Han-Sheng Chuang: Conceptualization, Project administration, Supervision, Funding acquisition, Writing – original draft, Writing – review & editing. **Wei-Long Chen:** Investigation, Methodology, Data curation, Formal analysis, Writing – original draft, Writing – review & editing. **Chun-Jui Chen & Chun-Chien Chang:** Investigation, Data curation, Writing – review & editing. **Tai-Hua Yang:** Project administration, Funding acquisition, Writing – review & editing.

Declaration of Competing Interest

The authors declare that they have no known competing financial interests or personal relationships that could have appeared to influence the work reported in this paper.

Data Availability

Data will be made available on request.

Acknowledgments

This research was supported by the Ministry of Science and Technology, Taiwan under the Grant 111-2221-E-006-066- and the Chi-Mei Medical Center under the collaborative Grant CMNCKU11001.

Appendix A. Supporting information

Supplementary data associated with this article can be found in the online version at doi:10.1016/j.sna.2022.113959.

References

[1] C.D. Meinhart, S.T. Wereley, J.G. Santiago, PIV measurements of a microchannel flow, Exp. Fluids 27 (1999) 414–419, https://doi.org/10.1007/s003480050366.
[2] J.G. Santiago, S.T. Wereley, C.D. Meinhart, D.J. Beebe, R.J. Adrian, A particle image velocimetry system for microfluidics, Exp. Fluids 25 (1998) 316–319, https://doi.org/10.1007/s003480050235.
[3] C.D. MeinhartH. Zhang, The flow structure inside a microfabricated inkjet printhead, J. Microelectromech. Syst. 9 (2000) 67–75, https://doi.org/10.1109/84.825779.
[4] Y. Wei, T. Li, X. Zhou, Z. Zhang, Time-resolved measurement of the near-nozzle air entrainment of high-pressure diesel spray by high-speed micro-PTV technique, Fuel 268 (2020), 117343, https://doi.org/10.1016/j.fuel.2020.117343.
[5] W.-J. Kuo, Y.-S. Sie, H.-S. Chuang, Characterizations of kinetic power and propulsion of the nematode Caenorhabditis elegans based on a micro-particle image velocimetry system, Biomicrofluidics 8 (2014), 024116, https://doi.org/10.1063/1.4872061.
[6] J. Zhou, P.-L. Lee, C.-S. Tsai, C.-I. Lee, T.-L. Yang, H.-S. Chuang, W.-W. Lin, T.-E. Lin, S.H. Lim, S.-Y. Wei, Y.-L. Chen, S. Chien, J.-J. Chiu, Force-specific activation of Smad1/5 regulates vascular endothelial cell cycle progression in response to disturbed flow, Proc. Natl. Acad. Sci. USA 109 (2012) 7770–7775, https://doi.org/10.1073/pnas.1205476109.
[7] G. Silva, V. Semiao, N. Reis, Rotating microchannel flow velocity measurements using the stationary micro-PIV technique with application to lab-on-a-CD devices, Flow Meas. Instrum. 67 (2019) 153–165, https://doi.org/10.1016/j.flowmeasinst.2019.04.001.
[8] J.W. Van der Kindere, A. Laskari, B. Ganapathisubramani, R. de Kat, Pressure from 2D snapshot PIV, Exp. Fluids 60 (2019) 32, https://doi.org/10.1007/s00348-019-2678-5.
[9] H. Kinoshita, M. Oshima, J. Hong, T. Fujii, T. Saga, T. Kobayashi, PIV measurement of pressure- and electrokinetically-driven flow in microchannels. Optical Technology and Image Processing for Fluids and Solids Diagnostics, SPIE, 2002, p. 2003.
[10] L. Qin, J. Hua, X. Zhao, Y. Zhu, D. Li, Z. Liu, Micro-PIV and numerical study on influence of vortex on flow and heat transfer performance in micro arrays, Appl. Therm. Eng. 161 (2019), 114186, https://doi.org/10.1016/j.applthermaleng.2019.114186.
[11] S.A. Vagner, S.A. Patlazhan, C.A. Serra, D. Funfschilling, Vortex flow evolution in a growing microdroplet during co-flow in coaxial capillaries, Phys. Fluids 33 (2021), 072010, https://doi.org/10.1063/5.0057353.
[12] H.J. Kim, Measurements of temperature and flow fields with sub-millimeter spatial resolution using two-color laser induced fluorescence (LIF) and micro-particle image velocimetry (PIV), J. Mech. Sci. Technol. 19 (2005) 716–727, https://doi.org/10.1007/BF02916193.
[13] Y.-S. SieH, -S. Chuang, A micro-volume viscosity measurement technique based on μPIV diffusometry, Microfluid. Nanofluid. 16 (2014) 65–72, https://doi.org/10.1007/s10404-013-1219-4.
[14] K.N. Clayton, D. Lee, S.T. Wereley, T.L. Kinzer-Ursem, Measuring biotherapeutic viscosity and degradation on-chip with particle diffusometry, Lab Chip 17 (2017) 4148–4159, https://doi.org/10.1039/C7LC00507E.
[15] H.-S. Chuang, W.-J. Kuo, C.-L. Lee, I.H. Chu, C.-S. Chen, Exercise in an electrotactic flow chamber ameliorates age-related degeneration in Caenorhabditis elegans, Sci. Rep. 6 (2016) 28064, https://doi.org/10.1038/srep28064.
[16] J. Lafaurie-Janvore, E. Antoine, S. Perkins, A. Babataheri, A. Barakat, A simple microfluidic device to study cell-scale endothelial mechanotransduction, Biomed. Microdevices 18 (2016) 63, https://doi.org/10.1007/s10544-016-0090-y.
[17] N. Van Toan, T.T.K. Tuoi, Y.-C. Tsai, Y.-C. Lin, T. Ono, Micro-fabricated presure sensor using 50 nm-thick of Pd-based metallic glass freestanding membrane, Sci. Rep. 10 (2020) 10108, https://doi.org/10.1038/s41598-020-67150-y.
[18] T. Kim, A. Saini, J. Kim, A. Gopalarathnam, Y. Zhu, F.L. Palmieri, C.J. Wohl, X. Jiang, Piezoelectric floating element shear stress sensor for the wind tunnel flow measurement, IEEE Trans. Ind. Electron. 64 (2017) 7304–7312, https://doi.org/10.1109/tie.2016.2630670.
[19] X. Wang, Z. Fang, X. Song, W. Xu, A nanoscale hot-wire flow sensor based on CMOS-MEMS technology, Front. Mech. Eng. 8 (2022), 877754, https://doi.org/10.3389/fmech.2022.877754.
[20] Q. Yu, Z. Xu, J. Zhao, M. Zhang, X. Ma, PIV-based acoustic pressure measurements of a single bubble near the elastic boundary, Micromachines 11 (2020) 637, https://doi.org/10.3390/mi11070637.
[21] P. Chamarthy, S.V. Garimella, S.T. Wereley, Non-intrusive temperature measurement using microscale visualization techniques, Exp. Fluids 47 (2009) 159–170, https://doi.org/10.1007/s00348-009-0646-1.
[22] A. Charogiannis, I. Zadrazil, C.N. Markides, Thermographic particle velocimetry (TPV) for simultaneous interfacial temperature and velocity measurements, Int. J. Heat Mass Transf. 97 (2016) 589–595, https://doi.org/10.1016/j.ijheatmasstransfer.2016.02.050.
[23] C.-J. Chen, W.-L. Chen, P.H. Phong, H.-S. Chuang, Investigation of micro-volume viscosity with Janus microbeads based on rotational brownian motion, Sensors 19 (2019) 1217, https://doi.org/10.3390/s19051217.
[24] W.-L. ChenH, -S. Chuang, Development of a self-viscosity and temperature-compensated technique for highly stable and highly sensitive bead-based diffusometry, Biosensors 12 (2022) 362, https://doi.org/10.3390/bios12060362.

[25] T. Ishida, K. Maekawa, T. Kishi, Enhanced modeling of moisture equilibrium and transport in cementitious materials under arbitrary temperature and relative humidity history, Cem. Concr. Res. 37 (2007) 565–578, https://doi.org/10.1016/j.cemconres.2006.11.015.
[26] W.-L. ChenH, -S. Chuang, Trace biomolecule detection with functionalized Janus particles by rotational diffusion, Anal. Chem. 92 (2020) 12996–13003, https://doi.org/10.1021/acs.analchem.0c01733.
[27] C. Bourdon, M. Olsen, A. Gorby, The depth of correlation in micro-PIV for high numerical aperture and immersion objectives, J. Fluids Eng. 128 (2006) 883–886, https://doi.org/10.1115/1.2201649.

Jhih-Cheng Wang is a medical doctor in the Department of Urology at Chimei Medical Center, Tainan, Taiwan. He is also a joint assistant professor in the Center for General Education at Southern Taiwan University of Science and Technology, Tainan, Taiwan.

Wei-Long Chen is a Ph.D. student in the Department of Biomedical Engineering at National Cheng Kung University, Tainan, Taiwan.

Chun-Jui Chen is a Ph.D. student in the Department of Biomedical Engineering at National Cheng Kung University, Tainan, Taiwan.

Chun-Chien Chang is a graduate student in the Department of Biomedical Engineering at National Cheng Kung University, Tainan, Taiwan.

Tai-Hua Yang is currently a medical doctor in the Department of Orthopedic Surgery at National Cheng Kung University Hospital, Tainan, Taiwan. He is also an assistant professor in the Department of Biomedical Engineering at National Cheng Kung University, Tainan, Taiwan. His research interests focus on orthopedics, image processing, medical devices, and molecular biology.

Han-Sheng Chuang is currently a full professor in the Department of Biomedical Engineering at National Cheng Kung University, Tainan, Taiwan. His research interests focus on biomicrofluidics, MEMS/NEMS technology, optical diagnostics, and biomechanics of microorganisms.